Title
Glutamate Cysteine Ligase Modifier Subunit (Gclm) Null Mice Have Increased Ovarian Oxidative Stress and Accelerated Age-Related Ovarian Failure

Journal
Endocrinology, 156(9)

ISSN
0888-8809

Authors
Lim, Jinhwan
Nakamura, Brooke N
Mohar, Isaac
et al.

Publication Date
2015-09-01

DOI
10.1210/en.2015-1206

Glutamate Cysteine Ligase Modifier Subunit (*Gclm*) Null Mice Have Increased Ovarian Oxidative Stress and Accelerated Age-Related Ovarian Failure

Jinhwan Lim, Brooke N. Nakamura, Isaac Mohar, Terrance J. Kavanagh, and Ulrike Luderer

Departments of Medicine (J.L., B.N.N., U.L.) and Developmental and Cell Biology (U.L.), University of California Irvine, Irvine, California 92617; and Department of Environmental and Occupational Health Sciences (I.M., T.J.K.), University of Washington, Seattle, Washington 98195

Glutathione (GSH) is the one of the most abundant intracellular antioxidants. Mice lacking the modifier subunit of glutamate cysteine ligase (*Gclm*), the rate-limiting enzyme in GSH synthesis, have decreased GSH. Our prior work showed that GSH plays antiapoptotic roles in ovarian follicles. We hypothesized that $Gclm^{-/-}$ mice have accelerated ovarian aging due to ovarian oxidative stress. We found significantly decreased ovarian GSH concentrations and oxidized GSH/oxidized glutathione redox potential in $Gclm^{-/-}$ vs $Gclm^{+/+}$ ovaries. Prepubertal $Gclm^{-/-}$ and $Gclm^{+/+}$ mice had similar numbers of ovarian follicles, and as expected, the total number of ovarian follicles declined with age in both genotypes. However, the rate of decline in follicles was significantly more rapid in $Gclm^{-/-}$ mice, and this was driven by accelerated declines in primordial follicles, which constitute the ovarian reserve. We found significantly increased 4-hydroxynonenal immunostaining (oxidative lipid damage marker) and significantly increased nitrotyrosine immunostaining (oxidative protein damage marker) in prepubertal and adult $Gclm^{-/-}$ ovaries compared with controls. The percentage of small ovarian follicles with increased granulosa cell proliferation was significantly higher in prepubertal and 2-month-old $Gclm^{-/-}$ vs $Gclm^{+/+}$ ovaries, indicating accelerated recruitment of primordial follicles into the growing pool. The percentages of growing follicles with apoptotic granulosa cells were increased in young adult ovaries. Our results demonstrate increased ovarian oxidative stress and oxidative damage in young $Gclm^{-/-}$ mice, associated with an accelerated decline in ovarian follicles that appears to be mediated by increased recruitment of follicles into the growing pool, followed by apoptosis at later stages of follicular development. (***Endocrinology*** **156: 3329–3343, 2015)**

Reactive oxygen species (ROS) result from the sequential addition of electrons to molecular oxygen, forming superoxide anion radical, hydrogen peroxide, and hydroxyl radical. SO can also react with nitric oxide, forming peroxynitrite (1). ROS function as intracellular signaling molecules, but because they are highly reactive, they can damage important cellular components in the ovary and other tissues by reacting with lipids, proteins, and DNA (2). ROS and reactive nitrogen species are generated as byproducts of normal cellular processes such as oxidative phosphorylation. In steroid synthesizing tissues, such as the ovary and testis, ROS are generated due to uncoupling of electron transfer from substrate hydroxylation by steroidogenenic cytochrome P450 enzymes (3).

To prevent the adverse effects of high levels of ROS, the ovary possesses antioxidant defenses. Vitamins A, C, and

ISSN Print 0013-7227 ISSN Online 1945-7170
Printed in USA

Received March 3, 2015. Accepted June 12, 2015.
First Published Online June 17, 2015

Abbreviations: E_h, Nernst potential; FOXO, Forkhead box O; GCL, glutamate cysteine ligase; GCLC, catalytic subunit of GCL; GCLM, modifier subunit of GCL; GPX, glutathione peroxidase; GSH, glutathione; GSSG, oxidized glutathione; GST, glutathione-S-transferase; 4-HNE, 4-hydroxynonenal; NRF2, nuclear factor erythroid 2-related factor 2; NTY, nitrotyrosine; PCNA, proliferating cell nuclear antigen; PI3K, phosphatidylinositol-3-kinase; POF, premature ovarian failure; ROS, reactive oxygen species; SOD, superoxide dismutase; TSC, tuberous sclerosis complex; TUNEL, terminal deoxynucleotidyl transferase-mediated deoxyuridine 5-triphosphate nick end-labeling; UCI, University of California, Irvine; UW, University of Washington.

E, the antioxidant tripeptide glutathione (GSH), and ROS scavenging enzymes, such as superoxide dismutases (SOD), glutathione peroxidases (GPX), catalase, glutathione-S-transferases (GST), and peroxiredoxins are important for maintaining cellular redox poise (4–10). GSH is the most abundant intracellular nonprotein thiol and one of the most important intracellular antioxidants. GSH has numerous intracellular functions including reduction of hydrogen peroxide and lipid peroxides as a cofactor for GPXs and peroxiredoxin-6 and detoxification of electrophilic toxicants as a cofactor for GSTs (11). GSH is synthesized in two ATP-dependent reactions. The first, rate-limiting reaction is catalyzed by glutamate cysteine ligase (GCL), a heterodimer composed of a catalytic (GCLC) and a modifier (GCLM) subunit (12, 13). GCLC is responsible for the catalytic activity of the enzyme, whereas binding of GCLM to GCLC decreases the Michaelis constant for the substrates glutamate and ATP and increases the inhibitory constant for GSH (12, 13). *Gclm*, like *Gclc*, is ubiquitously expressed in all cells; however, the levels of *Gclm* expression and the relative expression of *Gclm* and *Gclc* vary among cell types (14, 15). In most tissues, GCLM is limiting for the synthesis of GSH (16). Although all cells have intracellular GSH concentrations in the millimolar range, oocytes have the highest intracellular GSH concentrations of any cell type (10 mM) (17).

Follicles are the functional unit of the ovary, consisting of the oocyte, surrounded by and communicating with specialized somatic cells, the granulosa and theca cells. Follicles progress from the least mature, quiescent primordial follicle stage through primary, secondary, and antral stages to mature preovulatory follicles. The vast majority of follicles does not survive to the preovulatory stage but undergoes a process of degeneration called atresia (18, 19). Due to atresia and ovulation, the number of follicles declines continuously throughout postnatal life, culminating in reproductive senescence, which normally occurs at 50 ± 4 years in women (20). Premature ovarian failure (POF) or primary ovarian insufficiency, which afflicts 1% of all women, is defined as cessation of ovarian function prior to the age of 40 years. Women with POF have premature depletion of the ovarian follicle reserve. The causes of POF are unknown in 90% of cases (21, 22). In recent years, several genetically modified mouse models have been described that experience POF. Among these are mice with the deletion of several genes in the phosphatidylinositol-3-kinase (PI3K)/AKT (also called protein kinase B) signaling pathway, including the inhibitor of the pathway phosphatase and tensin homolog deleted on chromosome 10 (*Pten*), phosphoinositide-dependent kinase (*Pdk1*), the targets of AKT phosphorylation tuberous sclerosis 1 and 2 (*Tsc1*, *Tsc2*), and the transcription factor *Foxo3a* (23–29). Mice null for *Pten*, *Tsc1/2*, and *Foxo3a* undergo rapid premature ovarian failure due to premature activation of primordial follicles followed by subsequent death of the activated follicles, whereas mice null for *Pdk1* undergo ovarian failure due to death of primordial follicles.

Our previous studies have shown that ovarian follicles and granulosa cells are sensitive to the initiation of apoptosis by stimuli that result in the generation of ROS (30–33). Furthermore, we have shown that oxidative protein, lipid, and DNA damage increase in mouse ovarian follicles and interstitial cells with normal aging, concomitant with a decline in ovarian expression of several antioxidant genes (34). Concentrations of GSH and expression of GSH-related genes are lower in oocytes from aged mice compared with those from young mice (35–37). ROS increase and antioxidant enzyme activities decrease with age in oocytes, follicular fluid, and/or cumulus cells of women undergoing assisted reproduction (38–40).

$Gclc^{-/-}$ mice die during embryonic development (11, 41, 42), whereas $Gclm^{-/-}$ mice survive and reproduce, despite greatly decreased tissue levels of GSH (11, 43, 44). We previously showed that female $Gclm^{-/-}$ mice have dramatically reduced fertility compared with wild-type littermates due to poor oocyte quality, causing preimplantation embryonic demise (45). Herein we tested the hypothesis that $Gclm^{-/-}$ females have low ovarian GSH concentrations, resulting in oxidative stress, oxidative damage, and accelerated age-related decline in ovarian follicles.

Materials and Methods

Materials

Chemicals and reagents were purchased from Fisher Scientific or Sigma-Aldrich unless otherwise noted.

Animals

$Gclm^{-/-}$ mice were generated by disrupting the *Gclm* gene by replacing exon 1 with a β-galactosidase/neomycin phosphotransferase fusion gene and were backcrossed onto a C57BL/6J genetic background (43, 46). Female mice for these experiments were generated at the University of California, Irvine (UCI) or the University of Washington (UW) by mating $Gclm^{+/-}$ males with $Gclm^{+/-}$ females. The mice were housed in American Association for the Accreditation of Laboratory Animal Care-accredited facilities, with free access to deionized water and laboratory chow (Harlan Teklad 2919; UCI; LabDiet 5053; UW), on a 14-hour light, 10-hour dark cycle (UCI) or on a 12-hour light, 12-hour light-dark cycle (UW). Temperature was maintained at 69–75°F. The experimental protocols were carried out in accordance with established guidelines (47) and were approved by the Institutional Animal Care and Use Committees at UCI and UW.

Estrous cycling

Estrous cycling in individually housed adult female mice was evaluated every morning for a minimum of 14 days by vaginal cytology (48, 49). *Gclm*$^{-/-}$ mice and wild-type littermates were euthanized by CO_2 narcosis followed by cardiac puncture (UCI) or followed by cervical dislocation (UW). For some end points, euthanasia occurred on defined days of the estrous cycle [metestrus for ovarian GSH concentrations and proestrus for ovarian immunohistochemistry and terminal deoxynucleotidyl transferase-mediated deoxyuridine 5-triphosphate nick end-labeling (TUNEL)].

Glutathione assays

Ovarian total and oxidized glutathione (GSSG) were measured using an enzymatic recycling assay with modifications as previously described (8, 50, 51). Reduced GSH concentrations were calculated from the total and oxidized glutathione concentrations.

The levels of GSH and GSSG decrease and increase, respectively, during oxidative stress. Therefore, the redox state of the GSH/GSSG redox couple is a useful indicator of oxidative stress. The ratio of GSH to GSSG is a commonly used indicator of the redox state of this couple. However, generally, two GSHs are oxidized for every GSSG formed. The Nernst potential (E_h) is a measure of the redox state for the GSH/GSSG redox couple that takes into account this stoichiometry. E_h was calculated as follows: $E_h = E_0 + (RT/nF)\ln[(GSSG)/(GSH)^2]$, where GSSG and GSH are molar concentrations calculated from the concentration in nanomoles per milligram protein, assuming a cellular volume of 5 μL/mg protein; R is the gas constant (8.314 J/mol · K); T is the absolute temperature (37°C = 310°K); n is the number of electrons transferred (two electrons in this case); F is Faraday's constant (96 485 Col/mol); E_0 is taken as −252 mV for pH 7.2, based on a value of −240 mV for pH 7.0, with an adjustment of −5.9 mV per 0.1 increase in pH (52, 53). The intracellular pH was assumed to be 7.2, based on prior studies in the ovary (54).

Immunostaining

Ovaries were fixed in 4% paraformaldehyde in PBS overnight at 4°C, cryoprotected in 15% sucrose in PBS, embedded in optimum cutting temperature compound, and cryosectioned at 10 μm thickness. For 4-hydroxynonenal (4-HNE), nitrotyrosine (NTY), cleaved caspase-3, and proliferating cell nuclear antigen (PCNA) immunostaining, antigen retrieval was performed at 95°C for 10–15 minutes using 10 mM citrate buffer. For 4-HNE, NTY, and cleaved caspase-3, immunostaining was carried out using the Vectastain ABC kit (PK-6101; Vector Laboratories) according to the manufacturer's instructions. PCNA immunostaining was performed using the Vector M.O.M. immunodection kit (PK-2200; Vector Laboratories) according to the manufacturer's instructions. All immunostaining procedures incorporated avidin/biotin and 3% hydrogen peroxide-blocking steps. Details regarding primary antibodies are provided in Table 1. Visualization was accomplished using 3′3′-diaminobenzidine chromogen substrate (Roche). Slides were counterstained with hematoxylin. The following negative controls were included in every experiment: secondary antibody without primary antibody; primary antibody without secondary antibody; and primary antibody replaced by rabbit IgG or mouse IgG, as appropriate for the primary antibody, with secondary antibody. For cleaved caspase-3, granulosa cells in atretic antral follicles served as internal positive controls. For PCNA, the granulosa cells of healthy secondary and antral follicles served as internal positive controls.

The numbers of 4-HNE, NTY, cleaved caspase-3, and PCNA-positive and -negative follicles were counted in 16–24 sections distributed throughout the ovary by an investigator (J.L.) blind to *Gclm* genotype. The percentages of positive primordial and primary follicles (containing one or more positive granulosa cells per largest cross-section) and secondary and antral follicles (containing three or more positive granulosa cells or theca cells per largest cross-section) were calculated and used for data presentation and analysis.

Terminal deoxynucleotidyl transferase-mediated deoxyuridine 5-triphosphate nick end-labeling

Ovaries were prepared for in situ detection of apoptosis using TUNEL as for immunostaining. TUNEL was carried out using the in situ cell death detection kit POD (Roche) as previously described (8, 55). Negative controls without terminal transferase and positive controls treated with deoxyribonuclease I were included in every experiment.

Numbers of TUNEL positive and negative secondary and antral follicles (containing three or more TUNEL positive granulosa cells per largest cross-section) were counted in 16–28 sections distributed throughout the ovary by an investigator (J.L.) blind to *Gclm* genotype. The percentages of TUNEL-positive secondary and antral follicles were calculated and used for the data presentation and analyses. Primordial and primary follicles almost never had TUNEL-positive cells.

Ovarian histomorphometry

Ovaries were fixed in Bouin's fixative for 24 hours at 4°C, washed four times in 50% ethanol, and stored in 70% ethanol until processing. Complete 5-μm serial sections were cut and stained with hematoxylin and eosin. Histological sections from each animal were evaluated by one of the investigators (U.L.) without knowledge of *Gclm* genotype for 2 day, 21 day, 3 month, 7 month, 9 month, and 12 month old mice and by another of the investigators (J.L.) for 2 month old mice. Ovarian follicles were classified as primordial (single layer of flattened granulosa cells), primary (single layer of cuboidal or mixed

Table 1. Antibody Table

Peptide/Protein Target	Antigen Sequence (if Known)	Name of Antibody	Manufacturer, Catalog Number, and/or Name of Individual Providing the Antibody	Species Raised (Monoclonal or Polyclonal)	Dilution Used
4-HNE protein adducts		Anti-4-HNE	Alpha Diagnostic, number HNE11-S	Rabbit; polyclonal	1:500
Proteins that are nitrated		Antinitrotyrosine	Millipore, number 06-284	Rabbit; polyclonal	1:50
PCNA p36		PCNA (PC10)	Santa Cruz Biotechnology, number SC-56	Mouse; monoclonal	1:1000
Activated caspase-3		Cleaved caspase-3 (Asp175) (5A1E)	Cell Signaling, number 9664	Rabbit; monoclonal	1:100

cuboidal/flattened granulosa cells), secondary (greater than one layer of granulosa cells), or antral (possessing an antral cavity or several fluid filled vesicles in the case of early antral follicles) (56, 57) and were further classified as healthy or atretic according to established criteria (18, 58). Primordial, primary, and secondary follicles, as well as naked oocytes in postnatal day 2 ovaries, were counted in every fifth serial section (59). The counts were multiplied times 5 to obtain estimates of the total number of follicles per ovary (60). Antral follicles were followed through every serial section, taking care to count each of these structures only once.

For the analysis of age-related changes in ovarian follicle numbers ovaries from several experiments were used. Ovaries from the postnatal day 2 and 21, 9-month, and 12-month time points were obtained from untreated mice; 9 and 12-month mice were killed on the morning of proestrus of the estrous cycle; 2- and 21-day-old mice were not yet cycling. Ovaries for the 3-month time point were collected from randomly cycling adult mice that had been treated 6 hours before euthanasia with 500 mg/kg acetaminophen or vehicle (46). Because initial analyses showed that acetaminophen treatment did not affect follicle numbers, data from both treated and control mice were pooled. Ovaries from 7.5-month-old mice were collected on the morning of estrus from the sesame oil vehicle control groups from our previously published study (61). The ovaries for the analysis of ovarian follicle counts at 2 months of age were collected on the morning of proestrus (see Figure 7, A–D); these data are presented separately because the experiment was performed more than 3 years after the other experiments.

Serum LH and FSH assays

Pituitary panel multiplex kits (EMD Millipore) were used to measure LH and FSH concentrations in serum of 2-month-old *Gclm*$^{-/-}$ and *Gclm*$^{+/+}$ mice euthanized between 9:00 AM and 12:00 PM on proestrus. These assays were performed at the University of Virginia Center for Research in Reproduction Ligand Assay and Analysis Core. The laboratory intra- and interassay coefficients of variation for this assay were 5.5% and 11.5%, respectively.

Statistical analyses

For continuous variables, the Levene's test was used to test for homogeneity of variances. The effects of *Gclm* genotype on various end points were analyzed by independent-samples *t* test for equal or unequal variances as appropriate. Quantities expressed as fractions were subjected to arcsine square root transformation prior to the *t* test (62) or were analyzed by the nonparametric Mann-Whitney test. Analyses of the combined effects of age and genotype used two-way ANOVA. Differences in the distribution of regular and irregular estrous cycles by genotype were assessed using the Pearson χ^2 statistic. Data are presented as mean ± SEM in the figures and tables. Statistical analyses were performed using SPSS 20.0 for Mac OS X (IBM Software).

Results

Decreased GSH and GSSG concentrations and oxidized GSH redox potential in *Gclm*$^{-/-}$ ovaries

Gclm$^{-/-}$ females had significantly decreased ovarian total GSH and GSSG concentrations compared with

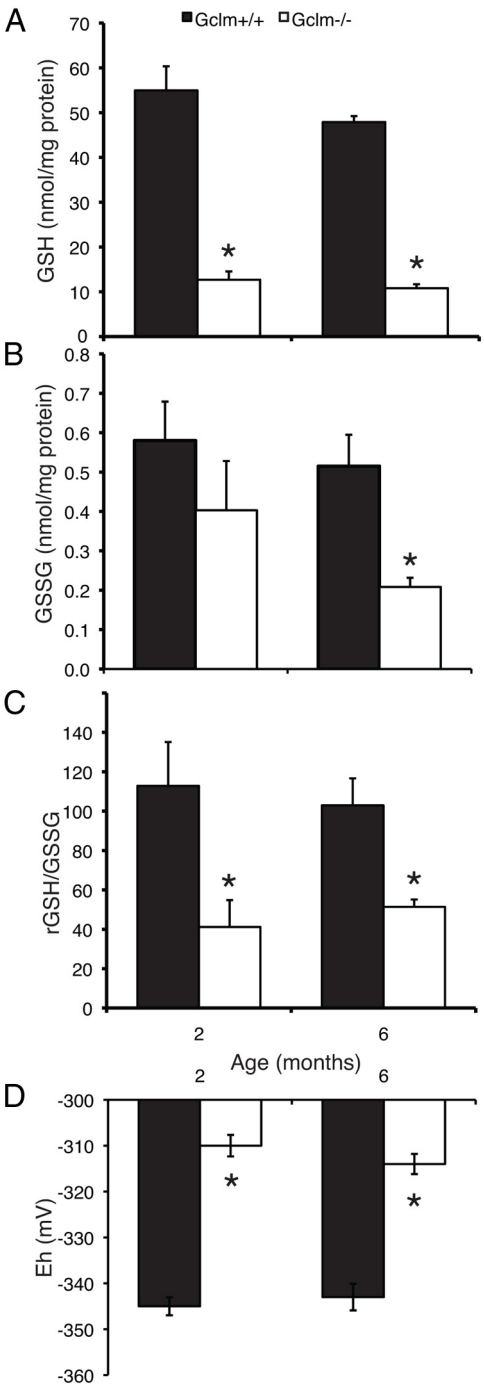

Figure 1. *Gclm*$^{-/-}$ mice have greatly decreased ovarian concentrations of total GSH and oxidized GSH/GSSG redox state compared with wild-type littermates. Total and oxidized GSH were measured; the ratio of GSH to GSSG and the E_h for GSH/GSSG were calculated as described in *Materials and Methods*. A, Mean ± SEM of total ovarian GSH at 2 and 6 months of age. *, $P < .001$ compared with *Gclm*$^{+/+}$ of the same age by *t* test. B, Mean ± SEM of ovarian GSSG concentrations at 2 and 6 months of age. *, $P = .008$ compared with *Gclm*$^{+/+}$ of the same age by *t* test. C, Mean ± SEM of GSH to GSSG ratio. *, $P < .03$ compared with *Gclm*$^{+/+}$ of the same age by *t* test. D, Mean ± SEM of E_h for GSH/GSSG redox couple. *, $P \leq .002$ compared with *Gclm*$^{+/+}$ of the same age by *t* test.

Gclm$^{+/+}$ littermates. In both 2- and 6-month-old *Gclm*$^{-/-}$ females, ovarian GSH concentrations were 23% of *Gclm*$^{+/+}$ levels ($P < .001$ by *t* test at both ages; Figure 1A). GSSG concentrations were less decreased than total GSH in *Gclm*$^{-/-}$ ovaries, to 69% at 2 months ($P = .31$) and 40% at 6 months ($P = .008$), respectively, of *Gclm*$^{+/+}$ levels (Figure 1B). The ratio of reduced GSH to GSSG was decreased significantly by approximately half in *Gclm*$^{-/-}$ females compared with *Gclm*$^{+/+}$ females at both ages (Figure 1C; $P = .021$ and $P = .009$, respectively), and the Nernst potential (E_h) for the GSH/GSSG redox couple was significantly oxidized by about 30 mV in *Gclm*$^{-/-}$ females at both ages (Figure 1D; $P = .002$ and $P < .001$, respectively).

The age-related decline in ovarian follicles is accelerated in Gclm$^{-/-}$ mice

We hypothesized that the oxidative stress in *Gclm*$^{-/-}$ ovaries would cause accelerated depletion of ovarian fol-

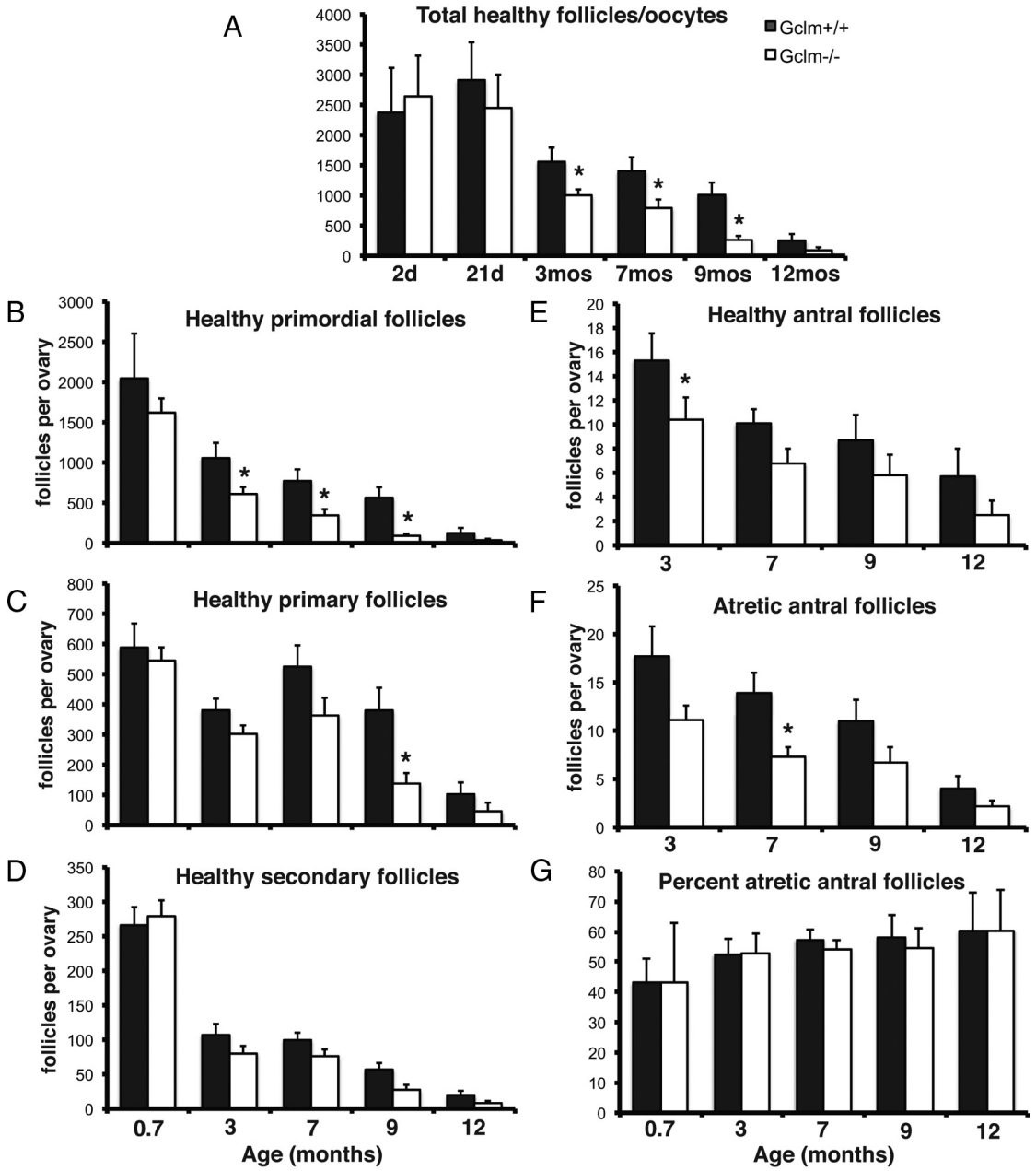

Figure 2. Accelerated age-related decline in ovarian follicles in *Gclm*$^{-/-}$ mice compared with wild-type littermates. Complete serial sections of ovaries were prepared and stained with hematoxylin and eosin, and healthy and atretic follicles were counted as described in *Materials and Methods*. A, Mean ± SEM of total numbers of healthy primordial plus primary plus secondary plus antral follicles in *Gclm*$^{+/+}$ and *Gclm*$^{-/-}$ ovaries at the indicated ages. B, Mean ± SEM of healthy primordial follicles. C, Mean ± SEM of healthy primary follicles. D, Mean ± SEM of healthy secondary follicles. E, Mean ± SEM of healthy antral follicles. F, Mean ± SEM of atretic antral follicles. G, Mean ± SEM percentage of atretic antral follicles. *, $P < .05$ compared with *Gclm*$^{+/+}$ of the same age.

licles compared with $Gclm^{+/+}$ ovaries. Total counts of healthy ovarian follicles and naked oocytes did not differ between $Gclm^{-/-}$ and $Gclm^{+/+}$ ovaries at postnatal day 2 or postnatal day 21, indicating that the initial complement of oocytes and packaging of oocytes into follicles is not disrupted by lack of *Gclm* (Figure 2A). Interestingly, very few antral follicles were observed in the 21-day-old $Gclm^{-/-}$ ovaries, whereas multiple antral follicles were present in the $Gclm^{+/+}$ ovaries, suggesting a delay in follicular development in the $Gclm^{-/-}$ ovaries.

The total number of ovarian follicles (primordial plus primary plus secondary plus antral) declined with age in both genotypes (Figure 2A). However, the rate of decline in healthy follicles was more rapid in $Gclm^{-/-}$ mice. By 3 months of age, $Gclm^{-/-}$ mice had 46% fewer follicles, by 7.5 months of age they had 54% fewer follicles, by 9 months they had 74% fewer follicles, and by 12 months they had 64% fewer follicles than $Gclm^{+/+}$ littermates ($P < .05$ for pairwise comparisons at 3, 7.5, and 9 mo by *t* test). This pattern of accelerated decline in $Gclm^{-/-}$ females compared with $Gclm^{+/+}$ females was recapitulated by the counts of healthy primordial follicles (Figure 2B; $P = .013$, effect of genotype overall; $P < .05$ for pairwise comparisons at 3, 7.5, and 9 mo by *t* test), indicating that their ovarian reserve was being depleted at a faster rate. Lower numbers of healthy follicles of all classes were observed in the $Gclm^{-/-}$ ovaries from adult mice from 3 months of age. The effect of *Gclm* genotype was statistically significant for primordial follicles, primary follicles, healthy antral follicles, and atretic antral follicles ($P < .03$; Figure 2, C–F), but most pairwise comparisons were not statistically significant. The effect of age was statistically significant for follicles of all classes ($P < .002$).

The numbers of atretic primordial, primary, and secondary follicles were very low, as we and others have previously reported (55, 63, 64), and did not differ by *Gclm* genotype (data not shown). The percentage of atretic antral follicles also did not differ by *Gclm* genotype (Figure 2G); it tended to increase with age in both genotypes, but the effect of age was not statistically significant ($P = .075$).

Age-related decline in estrous cycling in $Gclm^{-/-}$ and $Gclm^{+/+}$ mice

Estrous cycle data for $Gclm^{-/-}$ and $Gclm^{+/+}$ females are shown in Table 2. Most 2- and 6-month-old females of both genotypes had regular 4- to 5-day estrous cycles, with similar percentages of cornified vaginal cytology, characteristic of estrus, and leukocytic vaginal cytology, characteristic of metestrus and diestrus (Table 2). The 2-month-old $Gclm^{-/-}$ females had significantly longer estrous cycles than $Gclm^{+/+}$ females of the same age, which was associated with a significantly greater percentage of days with cornified vaginal cytology ($P < .05$). These genotype-related differences were not observed at other ages and may have occurred by chance. By 9 months of age, more animals of both genotypes had irregular cycles compared with younger mice. By 12 months, half of wild-type mice and 100% of $Gclm^{-/-}$ mice did not cycle at all. The difference in distribution of regular and irregular cycles between *Gclm* genotypes did not reach statistical significance at any age.

Ovarian oxidative damage is increased in $Gclm^{-/-}$ ovaries

We compared oxidative protein and lipid damage in ovaries of 21-day, 9-month, and 12-month-old $Gclm^{-/-}$ and $Gclm^{+/+}$ mice (Figures 3 and 4). As described above, at 21 days, no genotype-related differences in follicle numbers are observed, whereas at 9 and 12 months, $Gclm^{-/-}$ ovaries have fewer follicles than $Gclm^{+/+}$ ovaries. We found statistically significantly increased immunostaining for 4-HNE, a product of lipid peroxidation, in granulosa cells and theca cells of healthy secondary follicles in 21-day-old $Gclm^{-/-}$ ovaries, compared with $Gclm^{+/+}$ ova-

Table 2. Effects of *Gclm* Genotype on Estrous Cycles

		Age, mo			
	Genotype	**2**	**6**	**9**	**12**
Regular cycle, %[a]	$Gclm^{-/-}$	80	78	60	0
	$Gclm^{+/+}$	100	100	71	50
Leukocytic cytology, %	$Gclm^{-/-}$	45 ± 2	43 ± 2	32 ± 8	74 ± 10
	$Gclm^{+/+}$	43 ± 2	46 ± 2	45 ± 9	45 ± 13
Cornified cytology, %	$Gclm^{-/-}$	40 ± 2[b]	28 ± 2	55 ± 10	15 ± 8
	$Gclm^{+/+}$	31 ± 3	32 ± 3	35 ± 5	42 ± 13
Cycle length (days if cycling)	$Gclm^{-/-}$	5.2 ± 0.3[b]	4.3 ± 0.1	5.0 ± 1.0	NA
	$Gclm^{+/+}$	4.5 ± 0.2	4.2 ± 0.1	4.9 ± 0.4	6.4 ± 1.1

Abbreviation: NA, not applicable, mice not cycling. Data are for n = 5–9/group.

[a] Percentage of mice having regular, 4- to 5-day estrous cycles.

[b] $P < .05$ vs $Gclm^{+/+}$ of same age by *t* test.

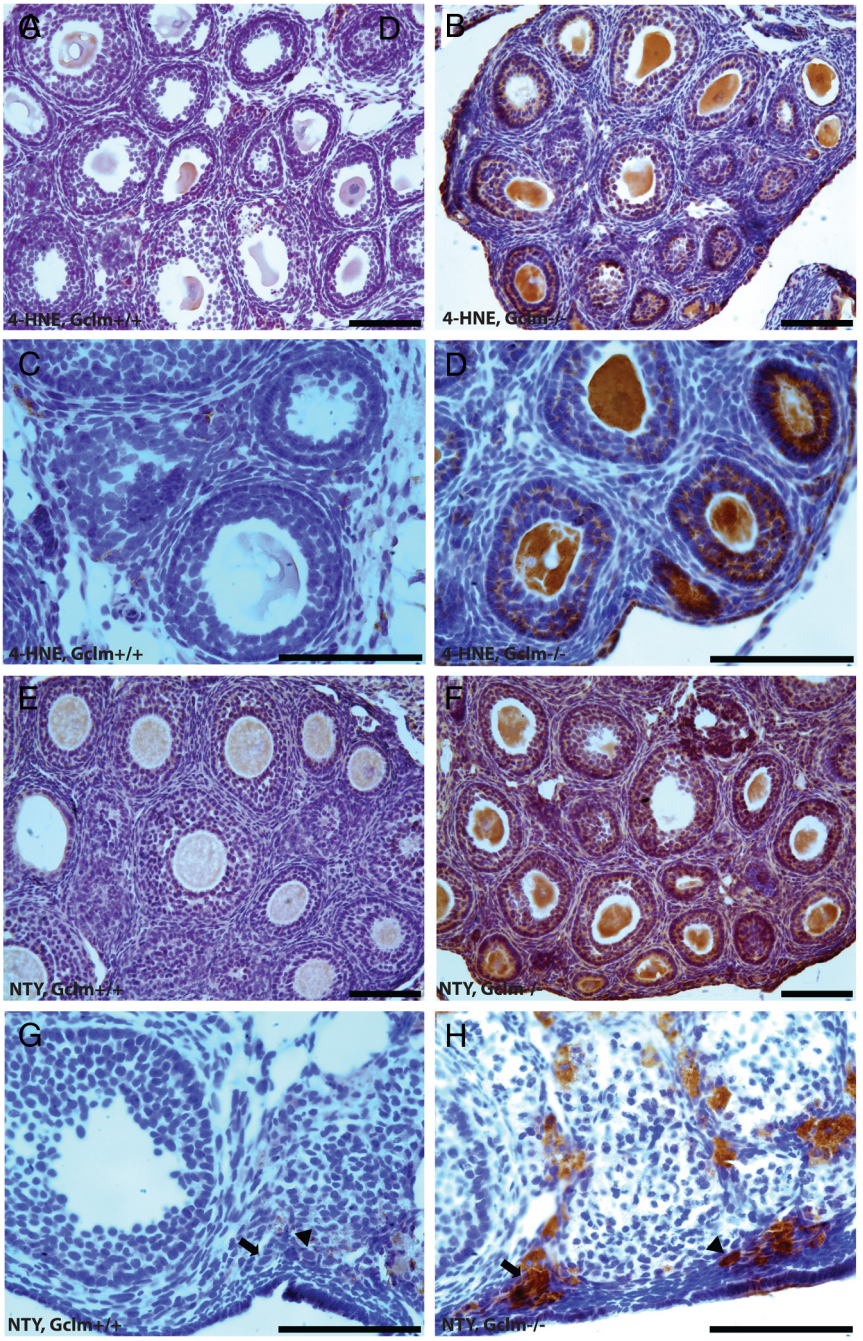

Figure 3. Ovarian oxidative damage in Gclm$^{-/-}$ mice. Ovarian oxidative damage in granulosa and theca cells was scored for immunostaining with oxidative damage markers as described in *Materials and Methods*. Representative images of immunostaining with each oxidative damage marker in the granulosa and theca cells are as follows: lipid peroxidation (4-HNE; A–D) and protein NTY (E–H) in the ovaries of 21-day- and 9-month-old *Gclm*$^{+/+}$ and *Gclm*$^{-/-}$ mice. A, Representative image of immunostaining for 4-HNE in the ovary of a 21-day-old *Gclm*$^{+/+}$ mouse. B, Representative image of immunostaining for 4-HNE in the ovary of a 21-day-old *Gclm*$^{-/-}$ mouse. C, Representative image of immunostaining for 4-HNE in the ovary of a 21-day-old *Gclm*$^{+/+}$ mouse. D, Representative image of immunostaining for 4-HNE in the ovary of a 21-day-old *Gclm*$^{-/-}$ mouse. E, Representative image of immunostaining for NTY in the ovary of a 21-day-old *Gclm*$^{+/+}$ mouse. F, Representative image of immuonstaining for NTY in the ovary of a 21-day-old *Gclm*$^{-/-}$ mouse. G, Representative image of immunostaining for NTY in the ovary of a 9-month-old *Gclm*$^{+/+}$ mouse. The black arrows indicate primary follicles and the black arrowheads indicate primordial follicles. H, Representative image of immunostaining for NTY in the ovary of a 9-month-old *Gclm*$^{-/-}$ mouse. All scale bars, 100 μm.

ries ($P = .019$ and $P = .011$, respectively, by Mann-Whitney test; Figures 3, A–D, and 4, E and G). There were no statistically significant differences in 4-HNE immunostaining in healthy primordial and primary follicles ($P = .280$ and $P = .051$, respectively, by Mann-Whitney test for primary follicles; Figures 3, C and D, and 4, A and C). Although the increased percentage of antral follicles with 4-HNE-positive theca cells in 9-month-old *Gclm*$^{-/-}$ ovaries approached significance ($P = .065$), no statistically significant *Gclm* genotype-related differences in 4-HNE immunostaining were found in ovaries from 9-month-old mice (Figure 4, A, C, E, G, I, and K).

We found increased immunostaining for NTY in granulosa cells of primary follicles in 21-day-old and 9-month *Gclm*$^{-/-}$ ovaries compared with *Gclm*$^{+/+}$ ovaries ($P = .039$ and $P = .008$, respectively; Figures 3, E and F, and 4D). The percentage of NTY-positive primordial follicles was also statistically significantly higher in 9-month-old *Gclm*$^{-/-}$ compared with *Gclm*$^{+/+}$ ovaries ($P = .033$; Figure 4B). No statistically significant genotype-related differences in NTY immunostaining were observed for secondary or antral follicles in ovaries from 21-day-old or 9-month-old mice (Figure 4, F, H, J, and L).

Very few follicles of any stage were found in 12-month-old ovaries of either *Gclm* genotype, and therefore, *Gclm* genotype-related differences in 4-HNE or NTY immunostaining could not be detected at this age (data not shown).

Ovarian follicular activation is increased in *Gclm*$^{-/-}$ ovaries

PCNA immunostaining was used as a marker of proliferation of granulosa cells (Figure 5). In ovaries from 21-day-old mice, the percentage of

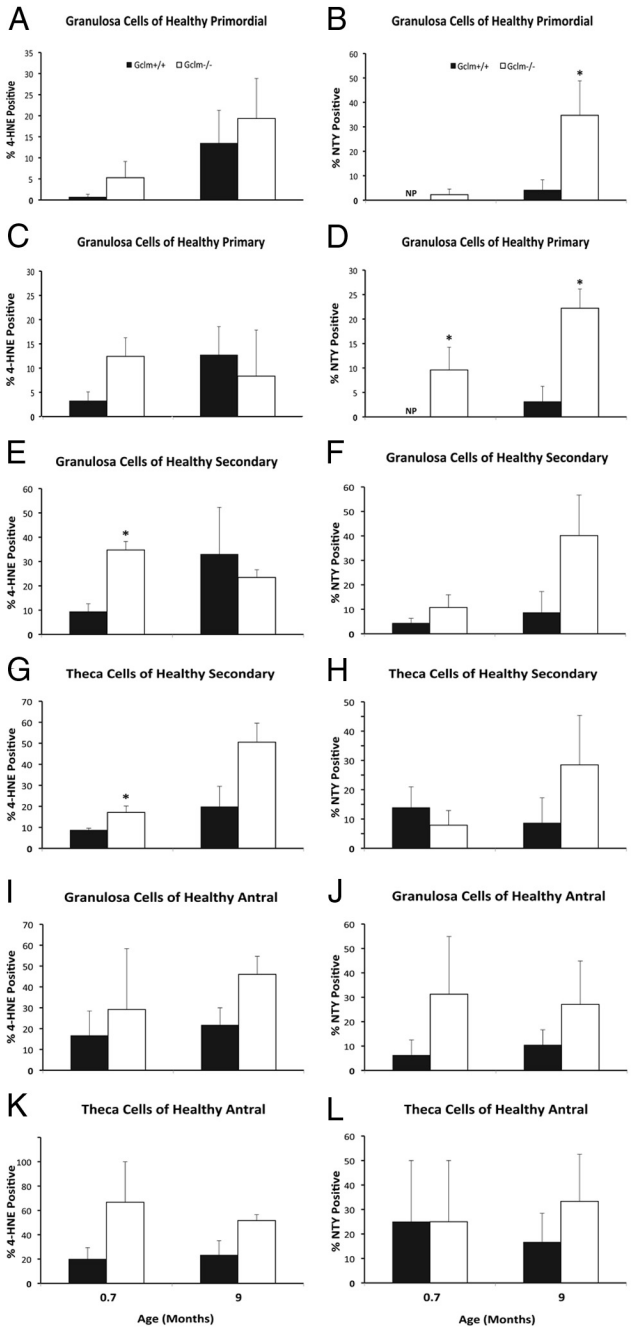

Figure 4. Increased ovarian oxidative damage in $Gclm^{-/-}$ mice. Ovarian oxidative damage in granulosa and theca cells of 21-day (0.7 months) and 9-month-old mice was scored for immunostaining with oxidative damage markers as described in *Materials and Methods*. Quantification of immunostaining with each oxidative damage marker in granulosa cells of healthy primordial follicles are as follows: A, lipid peroxidation (4-HNE); B, protein NTY. C and D, Quantification of immunostaining with each oxidative damage marker in granulosa cells of healthy primary follicles as follows: C, 4-HNE; D, NTY. E and F, Quantification of immunostaining with each oxidative damage marker in granulosa cells of healthy secondary follicles as follows: E, 4-HNE; F, NTY. G and H, Quantification of immunostaining with each oxidative damage marker in theca cells of healthy secondary follicles as follows: G, 4-HNE; H, NTY. I and J, Quantification of immunostaining with each oxidative damage marker in granulosa cells of healthy antral follicles as follows: I, 4-HNE; J, NTY. K and L, Quantification of immunostaining with each oxidative damage marker in theca cells of healthy antral follicles as follows: K, 4-HNE; L, NTY. NP, no follicles scored positive for the given marker. Data presented are means ± SEM of the percentage of follicles with positive staining for the indicated marker from three or five experiments. Statistical significance was analyzed using an independent-samples *t* test after arcsine square root transformation and nonparametric Mann-Whitney *U* test; the results of both tests were similar. *, Significant difference between genotypes at $P < .05$ (n = 4–6/group).

primordial and secondary follicles with PCNA-positive granulosa cells did not differ by *Gclm* genotype, but the percentage of PCNA-positive primary follicles was significantly higher in $Gclm^{-/-}$ ovaries than in $Gclm^{+/+}$ ovaries ($P = .020$). Our follicle classification scheme placed transitional or activated follicles into the same group as primary follicles. Therefore, the increase in PCNA-positive primary follicles is indicative of increased recruitment of primordial follicles into the growing pool.

There were so few primordial or primary follicles in the remaining sections from 9- and 12-month-old mice that no conclusions could be drawn about the effects of *Gclm* genotype on granulosa cell PCNA immunostaining at those ages.

The percentages of healthy primordial and primary follicles out of total healthy ovarian follicles are shown in Figure 6, A and B, respectively, for 21-day, 3-month, 7.5-month, and 9-month-old mice. These graphs show that beginning at 3 months of age, the percentage of primordial follicles decreased, whereas the percentage of primary follicles increased in $Gclm^{-/-}$ compared with $Gclm^{+/+}$ ovaries. The differences in primordial follicle percentages between the *Gclm* genotypes were statistically significant at 7.5 and 9 months of age, whereas the differences in primary follicle percentages were statistically significant at 7.5 months and approached significance at 3 months ($P = .08$). These data provide additional support for accelerated recruitment of primordial follicles into the growing pool in $Gclm^{-/-}$ ovaries and further suggest that this may increase with age.

Effects of *Gclm* deletion on ovarian follicle counts, apoptosis, proliferation, and oxidative damage at 2 months of age

Having identified the period between 21 days and 3 months of age as the critical window when $Gclm^{-/-}$ and $Gclm^{+/+}$ ovaries begin to show differences, we performed a detailed analysis of the effects of *Gclm* genotype on ovaries harvested on the day of proestrus at 2 months of age. The numbers of healthy primordial ($P = .113$), primary ($P = .202$), secondary ($P = .185$), and antral ($P = .058$) follicles were nonsignificantly lower in $Gclm^{-/-}$ ovaries than in $Gclm^{+/+}$ ovaries (Figure 7A). The percentage of

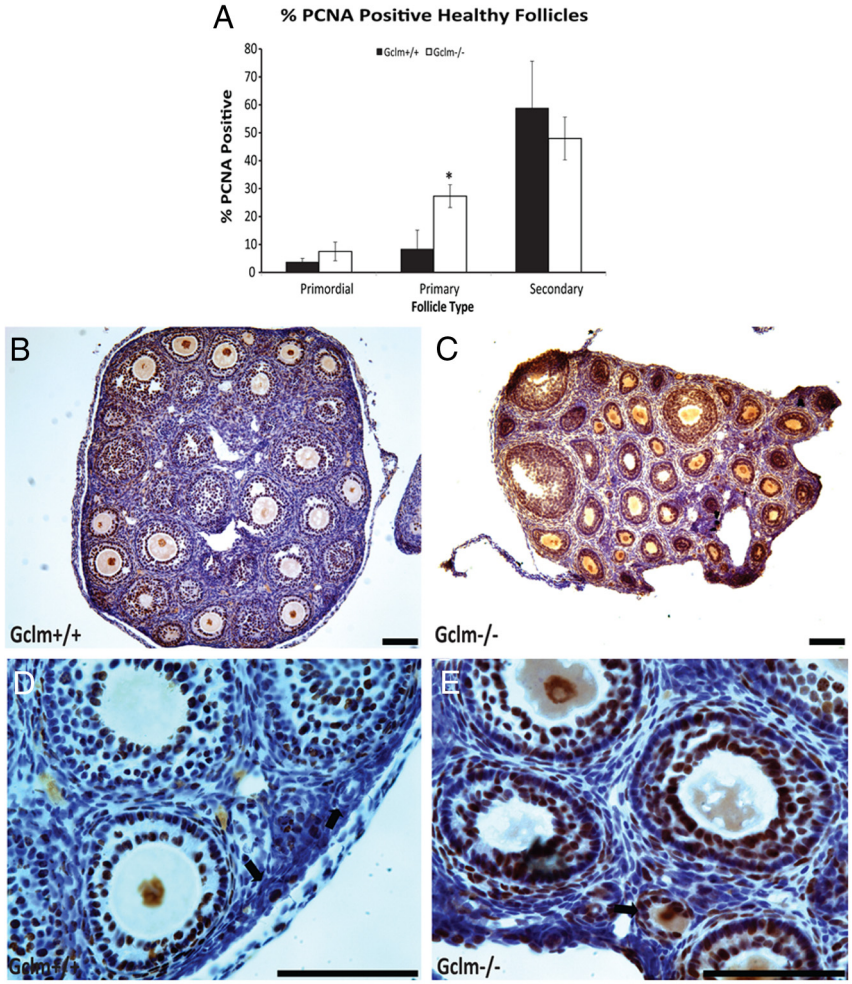

Figure 5. Increased granulosa cell proliferation in *Gclm*$^{-/-}$ mouse ovaries. Granulosa cell proliferation was scored as immunostaining with PCNA as described in *Materials and Methods*. A, Quantification of immunostaining with PCNA in granulosa cells of healthy primordial, primary, and secondary follicles in 21-day-old female mice. *, Significant difference with genotype at $P < .05$ (n = 4–6/group). B, Representative image of immunostaining with PCNA in the ovary of 21-day-old *Gclm*$^{+/+}$ mice. C, Representative image of PCNA immunostaining in the ovary of 21-day-old *Gclm*$^{-/-}$ mice. D, Representative image of PCNA immunostaining in the ovary of 21-day-old *Gclm*$^{+/+}$ mice. E, Representative image of PCNA immunostaining in the ovary of 21-day-old *Gclm*$^{-/-}$ mice. The black arrows in D and E indicate primary follicles. Data presented are means ± SEM of the percentage of follicles with positive staining for PCNA from four experiments. Statistical significance was analyzed using an independent-samples *t* test after arcsine square root transformation. All scale bars, 100 μm.

primordial follicles was decreased and the percentage of primary follicles was increased, albeit nonsignificantly ($P = .147$ and $P = .073$, respectively), consistent with increased recruitment of primordial follicles into the growing pool (Figure 7B).

There were no *Gclm* genotype-related differences in serum concentrations of the gonadotropin hormones, LH (1.4 ± 0.3 ng/mL in *Gclm*$^{+/+}$ and 1.6 ± 0.4 ng/mL in *Gclm*$^{-/-}$) and FSH (57.6 ± 13.8 ng/mL in *Gclm*$^{+/+}$ and 37.3 ± 14.3 ng/mL in *Gclm*$^{-/-}$) on proestrus.

We performed cleaved caspase-3 immunostaining (Figure 7C) and TUNEL (Figure 7D) to detect apoptosis. We observed a significantly increased percentage of antral follicles with cleaved caspase-3-positive granulosa cells in 2-month-old *Gclm*$^{-/-}$ compared with *Gclm*$^{+/+}$ ovaries ($P = .047$; Figure 7C). We observed a nonsignificantly higher percentage of cleaved caspase 3-positive secondary follicles at 2 months of age in *Gclm*$^{-/-}$ ovaries ($P = .108$; Figure 7C). The percentage of secondary follicles with TUNEL-positive granulosa cells was significantly higher at 2 months of age in *Gclm*$^{-/-}$ ovaries than in *Gclm*$^{+/+}$ ovaries ($P = .028$), whereas there was no statistically significant difference in the percentages of TUNEL-positive antral follicles between *Gclm*$^{-/-}$ and *Gclm*$^{+/+}$ ovaries (Figure 7D). The percentage of secondary follicles with 4-HNE-positive granulosa cells was significantly higher in 2-month-old *Gclm*$^{-/-}$ ovaries compared with *Gclm*$^{+/+}$ ovaries ($P = .032$, Figure 7F), whereas there were no differences in the percentage of 4-HNE-positive antral follicles (data not shown). We observed a significantly increased percentage of primary follicles with PCNA-positive, proliferating granulosa cells at 2 months of age in *Gclm*$^{-/-}$ compared with *Gclm*$^{+/+}$ ovaries ($P = .032$; Figure 7E).

We also performed TUNEL analysis on ovaries from the same 21-day and 9-month-old mice for which data on follicle counts, oxidative damage, and proliferation were presented above (Supplemental Figure 1A). Overall, there were no statistically significant *Gclm* genotype-related differences in the percentages of TUNEL-positive secondary or antral follicles at 21 days of age or 9 months of age. The apparent increase in TUNEL-positive secondary follicles in *Gclm*$^{-/-}$ null ovaries at 21 days of age was not statistically significant ($P = .19$).

We observed very few cleaved caspase-3- or TUNEL-positive primordial or primary follicles, and there were no apparent effects of *Gclm* genotype on these endpoints (data not shown).

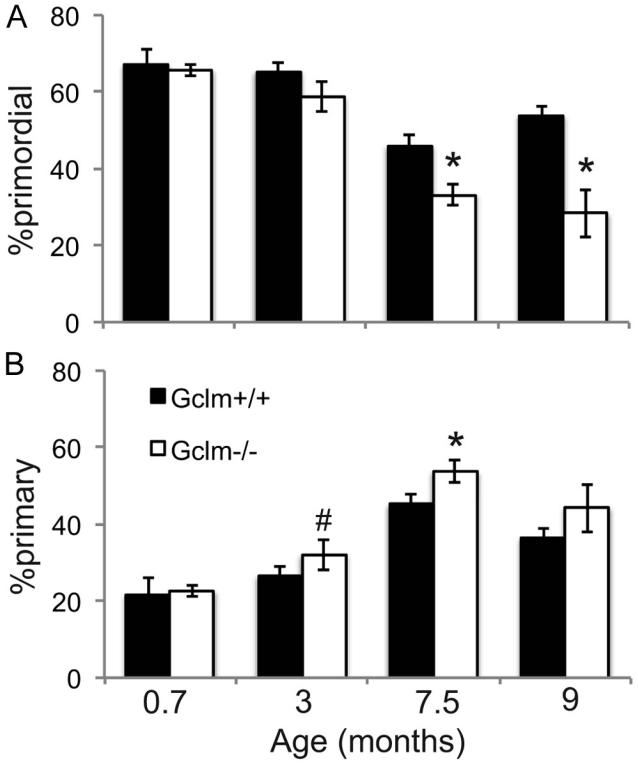

Figure 6. Increased primordial follicle activation in $Gclm^{-/-}$ mice. These graphs show the mean ± SEM percentage of healthy primordial follicles (A) or primary follicles (B) of total healthy follicles (calculated from counts shown in Figure 2, A and B). *, $P < .05$ by *t* test compared to $Gclm^{+/+}$ ovaries of the same age; #, $P = .08$ compared with $Gclm^{+/+}$ ovaries of the same age.

Discussion

Our results demonstrate that $Gclm^{-/-}$ mice have greatly decreased ovarian GSH concentrations, decreased ratio of GSH to GSSG, and oxidized E_h of the GSH/GSSG redox couple compared with $Gclm^{+/+}$ littermates, consistent with chronic ovarian oxidative stress. Further demonstrating ovarian oxidative stress, $Gclm^{-/-}$ ovaries show increased lipid peroxidation and protein oxidation by immunostaining for 4-HNE and NTY, respectively. Moreover, $Gclm^{-/-}$ and $Gclm^{+/+}$ females are born with an equal complement of oocytes, but $Gclm^{-/-}$ females experience an accelerated age-related decline in primordial follicles. Increased oxidative damage was observed in the $Gclm^{-/-}$ ovaries at 21 days of age, before any difference in follicle numbers, suggesting that oxidative stress may be driving the accelerated decline in ovarian follicles in $Gclm^{-/-}$ mice. Moreover, immunostaining for the proliferation marker PCNA showed that $Gclm^{-/-}$ ovaries had increased proliferation in primary follicles at 21 days of age, consistent with increased recruitment of quiescent primordial follicles into the growing pool, followed by death of recruited follicles as a mechanism for accelerated follicle depletion in $Gclm^{-/-}$ mice. Consistent with the latter, at 2 months of age, markers of apoptosis, cell proliferation, and oxidative damage were increased in follicles of $Gclm^{-/-}$ ovaries compared with $Gclm^{+/+}$ ovaries, and by 3 months of age, a statistically significantly lower number of primordial follicles was observed in $Gclm^{-/-}$ ovaries, which accelerated with aging.

The 77% lower ovarian total GSH levels in $Gclm^{-/-}$ females compared with wild-type littermates in the present study is similar to the differences reported for cerebellar neurons and astrocytes (43) and somewhat less than differences reported for liver, kidney, and erythrocytes (44). The ratios of GSH to GSSG in liver, kidney, pancreas, and erythrocytes reportedly did not differ between $Gclm^{-/-}$ and $Gclm^{+/+}$ mice of unspecified sex (44), whereas the E_h of the GSSG/2GSH redox couple was oxidized by 40–90 mV in these tissues (11). We previously reported that the ratio of GSH to GSSG did not differ between $Gclm^{-/-}$ and $Gclm^{+/+}$ epididymides and was increased in testes of $Gclm^{-/-}$ males and that testicular spermatogenesis was normal in $Gclm^{-/-}$ males (65). In contrast, we observed that the GSH to GSSG ratio was decreased and the E_h of the GSSG/2GSH redox couple was oxidized in $Gclm^{-/-}$ compared with $Gclm^{+/+}$ ovaries. Taken together, these results suggest that the ovary is more susceptible to chronic oxidative stress caused by GSH deficiency compared with other tissues.

Although the magnitude of the GSH/GSSG ratio and E_h of the GSH/GSSG redox couple vary widely among tissues, significant age-related decreases in both GSH/GSSG and E_h occur in brain, liver, kidney, heart, eye, and testis of 26-month-old compared with 4-month-old male mice (66, 67). Furthermore, these age-related changes in the GSH/GSSG redox state are partially reversed by caloric restriction, which also prolongs the life span (66, 67). These prior data lead to the hypothesis that experimental manipulations that oxidize the GSH/GSSG redox state may accelerate aging, at least in some tissues/organs. Our data using mice genetically deficient in GSH synthesis, which have an oxidized ovarian GSH/GSSG redox state and accelerated ovarian aging, support this hypothesis.

Oxidative stress occurs when the production of ROS overwhelms antioxidant defense capacity in cells. Whereas oxidative damage in other organs has been extensively evaluated, relatively little information exists on oxidative damage in the ovary (2). We previously reported that aging in mice is associated with increased ovarian oxidative damage to DNA, protein, and lipids (34). We hypothesized that oxidative damage would be exacerbated in ovaries of $Gclm^{-/-}$ mice due to their decreased antioxidant capacity. Consistent with this hypothesis, we observed significantly increased immunostaining for 4-HNE in granulosa cells (21 d and 2 mo old) and theca

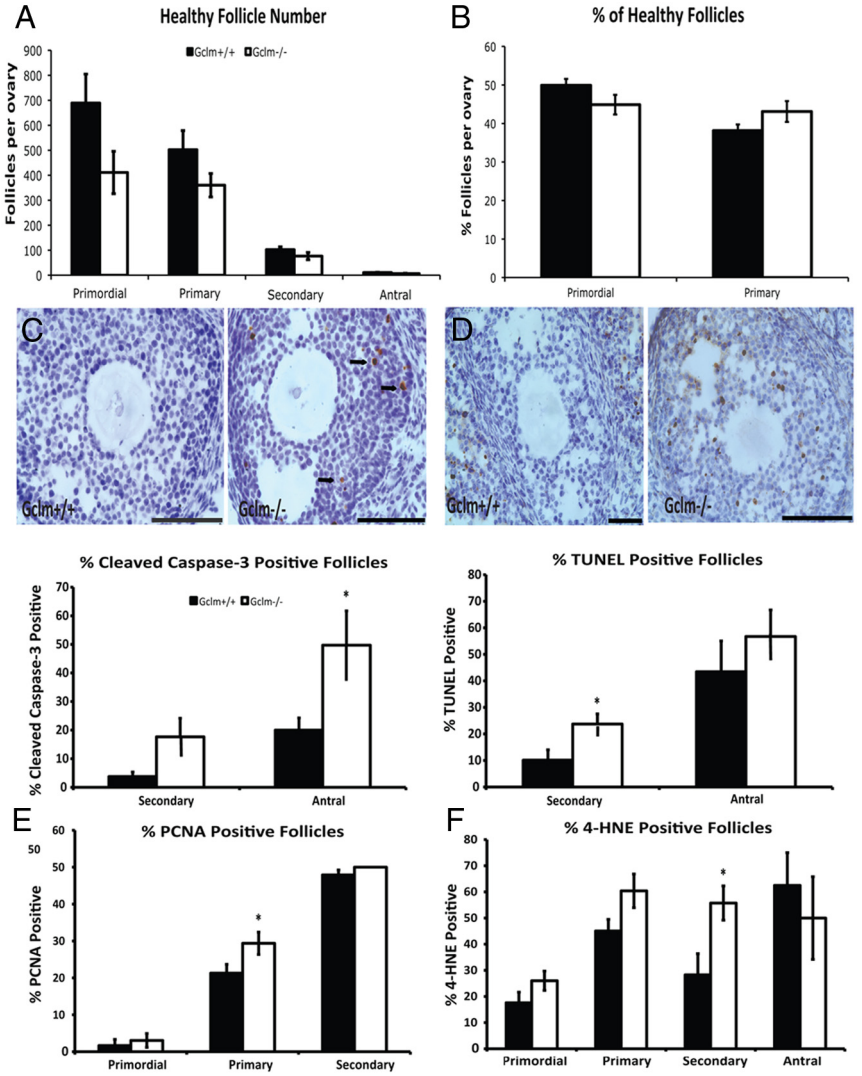

Figure 7. Effects of *Gclm* deletion on ovarian follicle counts, apoptosis, cell proliferation, and oxidative damage at 2 months of age. Healthy and atretic follicles were counted in hematoxylin and eosin-stained serial sections, as described in *Materials and Methods*. A, Mean ± SEM of numbers of healthy primordial, primary, secondary, and antral follicles in $Gclm^{+/+}$ and $Gclm^{-/-}$ ovaries at 2 months of age (n = 10 for $Gclm^{+/+}$ and n = 6 for $Gclm^{-/-}$). B, Mean ± SEM percentage of healthy primordial follicles and primary follicles of total healthy follicles (calculated from counts shown in Figure 7A). C and D, Cleaved caspase-3 and TUNEL were performed to detect apoptotic cells as described in *Materials and Methods*. C, Means ± SEM percentage of secondary and antral follicles that had cleaved caspase-3-positive granulosa cells (GC; n = 5/group). Representative images at top of caspase-3 immunostaining in $Gclm^{+/+}$ (left) and $Gclm^{-/-}$ (right) ovaries are shown. Black arrows indicate cleaved caspase-3-positive GCs of antral follicle. D, Means ± SEM of follicles with TUNEL-positive GCs in the ovaries of 2-month-old mice (n = 5/group). Representative images at top of TUNEL in $Gclm^{+/+}$ (left panel) and $Gclm^{-/-}$ (right panel) ovaries are shown. E and F, PCNA and 4-HNE were performed to detect proliferating GCs and oxidative damage as described in *Materials and Methods*. E, Means ± SEM percentage of primordial, primary, and secondary follicles with PCNA-positive GC (n = 5/group). F, Means ± SEM percentage of primordial, primary, secondary, and antral follicles with 4-HNE-positive GCs (n = 5/group). *, Significant difference between genotypes by nonparametric Mann-Whitney *U* test or *t* test at $P < .05$. All scale bars, 100 μm.

cells (21 d old) of healthy secondary follicles in $Gclm^{-/-}$ ovaries compared with $Gclm^{+/+}$ ovaries. 4-HNE is a product of lipid hydroperoxide decomposition by hydroxyl (or other) radical-mediated chain reactions in polyunsaturated fatty acids and lipoproteins (68, 69). The damage in membrane phospholipids decreases membrane fluidity, causing structural changes, and reduces activity of membrane-bound enzymes (68, 69).

Superoxide anion radical reacts with nitric oxide to generate peroxynitrite, forming NTY by nitration of tyrosine residues (70–72). NTY immunostaining is therefore a marker of oxidative protein damage. The percentage of NTY-positive primary follicles was higher in 21-day-old $Gclm^{-/-}$ ovaries and percentages of NTY-positive primordial and primary follicles were higher in 9-month-old $Gclm^{-/-}$ ovaries than in $Gclm^{+/+}$ ovaries. Our findings of oxidative damage to lipids and protein in young and middle-aged ovaries of $Gclm^{-/-}$ mice support the hypothesis that low GSH concentrations and oxidized GSH/GSSG redox potential in $Gclm^{-/-}$ ovaries result in increased oxidative stress-induced damage.

Importantly, the implications of this oxidative damage may be reflected in an increased rate of follicle turnover in $Gclm^{-/-}$ mice. PCNA is a marker of proliferating cells. As follicles are recruited into the growing pool, granulosa cells begin to proliferate. In ovaries from 21-day- and 2-month-old mice, we observed that the percentage of primary follicles with PCNA-positive staining was higher in $Gclm^{-/-}$ ovaries than in $Gclm^{+/+}$ ovaries. The increase in PCNA-positive primary follicles is indicative of increased recruitment of primordial follicles into the growing pool. Moreover, the increased recruitment of primordial follicles preceded the decline in ovarian follicle numbers, which was first observed at 3 months of age.

Consistent with increased primordial follicle recruitment in $Gclm^{-/-}$ mice, we also observed decreased percentages of primordial follicles at 2, 7.5, and 9 months of age and increased percentages of primary follicles at 2, 3, and 7.5 months of age in $Gclm^{-/-}$ compared with

Gclm$^{+/+}$ ovaries. Increased recruitment of primordial follicles into the growing pool may be driving the accelerated age-related follicle decline that we observed in *Gclm*$^{-/-}$ mice. Accelerated recruitment of primordial follicles into the growing pool with subsequent death of the prematurely activated follicles is responsible for premature ovarian failure in mice with oocyte-specific deletion of the PI3K/AKT signaling pathway genes *Pten*, *Tsc1*, *Tsc2*, and *Foxo3a* (23, 24, 26, 28) and in mice with global deletion of *Foxl2* (73, 74). ROS have been shown to promote phosphorylation (activation) of AKT and phosphorylation and acetylation of Forkhead box O (FOXO)-3a in nonovarian systems (75–77). We speculate that increased oxidative stress in the ovaries of *Gclm*$^{-/-}$ females may lead to the activation of AKT signaling, which inhibits tuberous sclerosis complex (TSC)-1, TSC2, and FOXO3a signaling, causing accelerated activation of primordial follicles.

Increases in activated (cleaved) caspase-3- and TUNEL-positive secondary and antral follicles in the present study are consistent with apoptosis of the prematurely activated follicles at later stages of follicular development in *Gclm*$^{-/-}$ mice. We observed minimal evidence for apoptosis or histological evidence of atresia in primordial follicles in mice of either *Gclm* genotype in the present study. However, we cannot exclude that primordial follicle death was occurring by a mechanism other than apoptosis, such as autophagy. Recent evidence suggests that autophagy may be an important cell death pathway in ovarian follicles (64, 78, 79). Future studies will examine the effects of *Gclm* deletion on autophagy in the ovary.

Few of the other genetically modified mouse models with deletion of antioxidant genes have been systematically evaluated for effects on ovarian function. Mice lacking the transcription factor nuclear factor erythroid 2-related factor 2 (NRF2) have decreased antioxidant capacity due to decreased basal and inducible transcription of antioxidant defense genes, including GSH synthesis genes (80, 81). *Nrf2*$^{-/-}$ female mice had significantly smaller litters than wild-type mice, but they did not have an accelerated decline in fertility with age (82). Female mice null for *Sod1* are also subfertile due to defects in the later stages of follicle maturation (83) and/or increased embryonic lethality (84). Copper chaperone for superoxide dismutase null mice, which have decreased ability to incorporate copper into SOD1, have a similar ovarian phenotype as *Sod1* null mice (85). Although *Sod2*$^{-/-}$ mice die before puberty, transplantation of *Sod2*$^{-/-}$ ovaries to wild-type hosts resulted in normal follicular development, ovulation, and viable offspring, suggesting that SOD2 is not required for normal ovarian function (83). Mice null for γ-glutamyl transpeptidase 1 (*Ggt1*) have female infertility, with lack of large antral follicles, corpora lutea, and ovulatory response to gonadotropins (86–88). *Ggt1*$^{-/-}$ mice have decreased ovarian cysteine concentrations and normal ovarian GSH concentrations compared with wild-type controls, and the female reproductive phenotype is completely rescued by cysteine replacement (86). Normal fertility has been reported in mice that lack *Gpx1* (89) or catalase (90).

In summary, *Gclm*$^{-/-}$ mice display low ovarian GSH levels, ovarian oxidative stress, and oxidative damage. Despite apparently normal in utero ovarian development, with normal complements of oocytes/ovarian follicles at birth and weaning, these mice subsequently experience an accelerated decline in ovarian follicles compared to wild-type littermates. Our data implicate accelerated recruitment of primordial follicles into the growing pool followed by apoptotic death of these follicles at later stages, rather than increased death of primordial follicles, as the driving force behind the accelerated follicle decline. Together with our previous work showing increasing ovarian oxidative damage and decreased antioxidant gene expression with aging, the present results provide strong evidence that ovarian oxidative stress plays a major role in ovarian aging.

Acknowledgments

We thank Reshma Patel, Jin Hur, Christine Pham, Angelica del Rosario, Jennifer Welch, Muzi Liu, and Chau Tran for their help with the mouse breeding and vaginal cytology. We also thank Honyin Chiu, Carrie Ng, and Sonia Maciejewski for their assistance with immunostaining and TUNEL.

Address all correspondence and requests for reprints to: Ulrike Luderer, MD, PhD, Center for Occupational and Environmental Health, 100 Theory Drive, Suite 100, Irvine, CA 92617. E-mail: uluderer@uci.edu.

Current address for B.N.N.: Norris Cancer Center, University of Southern California, 1441 Eastlake Avenue, Suite 3455, Los Angeles, CA 90003.

Current address for I.M.M.: Gradient, 600 Stewart Street, Suite 1900, Seattle, WA 98101.

This work was supported by National Institutes of Health (NIH) Grants R01ES020454, and R21AG032087 (to U.L.); NIH Grant P30CA062203 (to the University of California, Irvine, Chao Family Comprehensive Cancer Center); NIH Grants R01ES010849, P50ES015915, and P30ES007033 (to T.J.K.); NIH Grant T32ES007032 (to I.M.M.); the University of California, Irvine, Office of Research; the University of California, Irvine, Undergraduate Research Opportunities Program; and the University of California, Irvine, Center for Occupational and Environmental Health. The University of Virginia Center for Research in Reproduction Ligand Assay and Analysis Core is supported by the *Eunice Kennedy Shriver*

National Institute of Child Health and Human Development/ National Institutes of Health (National Centers for Translational Research in Reproduction and Infertility) Grant P50-HD28934.

Disclosure Summary: The authors have nothing to disclose.

References

1. **Radi R.** Peroxynitrite, a stealthy biological oxidant. *J Biol Chem*. 2013;288:26464–26472.
2. **Luderer U.** Ovarian toxicity from reactive oxygen species. In: Litwack G, ed. *Endocrine Disrupters*. Amsterdam: Academic Press/ Elsevier; 2014:99–127.
3. **Hanukoglu I.** Antioxidant protective mechanisms against reactive oxygen species (ROS) generated by mitochondrial P450 systems in steroidogenic cells. *Drug Metab Rev*. 2006;38:171–196.
4. **Sato EF, Kobuchi H, Edashige K, et al.** Dynamic aspects of ovarian superoxide dismutase isozymes during the ovulatory process in the rat. *FEBS Lett*. 1992;303:121–125.
5. **Hsieh CH, Tsai SP, Yeh HI, Sheu TC, Tam MF.** Mass spectrometric analysis of rat ovary and testis cytosolic glutathione S-transferases (GSTs): identification of a novel class-α GST, rGSTA6, in rat testis. *Biochem J*. 1997;323:503–510.
6. **Aten RF, Duarte KM, Behrman HR.** Regulation of ovarian antioxidant vitamins, reduced glutathione, and lipid peroxidation by luteinizing hormone and prostaglandin F_{2alpha}. *Biol Reprod*. 1992; 46:401–407.
7. **Gardiner CS, Salmen JJ, Brandt CJ, Stover SK.** Glutathione is present in reproductive tract secretions and improves development of mouse embryos after chemically induced glutathione depletion. *Biol Reprod*. 1998;59:431–436.
8. **Luderer U, Kavanagh TJ, White CC, Faustman EM.** Gonadotropin regulation of glutathione synthesis in the rat ovary. *Reprod Toxicol*. 2001;15:495–504.
9. **Tilly JL, Tilly KI.** Inhibitors of oxidative stress mimic the ability of follicle-stimulating hormone to suppress apoptosis in cultured rat ovarian follicles. *Endocrinology*. 1995;136:242–252.
10. **Mattison DR, Shiromizu K, Pendergrass JA, Thorgeirsson SS.** Ontogeny of ovarian glutathione and sensitivity to primordial oocyte destruction by cyclophosphamide. *Pediatr Pharmacol*. 1983;3:49–55.
11. **Dalton TP, Chen Y, Schneider SN, Nebert DW, Shertzer HG.** Genetically altered mice to evaluate glutathione homeostasis in health and disease. *Free Radic Biol Med*. 2004;37:1511–1526.
12. **Franklin CC, Backos DS, Mohar I, White CC, Forman HJ, Kavanagh TJ.** Structure, function, and post-translational regulation of the catalytic and modifier subunits of glutamate cysteine ligase. *Mol Aspects Med*. 2009;30:86–98.
13. **Griffith OW, Mulcahy RT.** The enzymes of glutathione synthesis: γ-glutamylcysteine synthetase. *Adv Enzymol Rel Areas Mol Biol*. 1999;73:209–267.
14. **Krzywanski DM, Dickinson DA, Iles KE, et al.** Variable regulation of glutamate-cysteine ligase subunit proteins affects glutathione biosynthesis in response to oxidative stress. *Arch Biochem Biophys*. 2004;423:116–125.
15. **Dahl EL, Mulcahy RT.** Cell-type specific differences in glutamate cysteine ligase transcriptional regulation demonstrate independent subunit control *Toxicol Sci*. 2001;61:265–272.
16. **Chen Y, Shertzer HG, Schneider SN, Nebert DW, Dalton TP.** Glutamate cysteine ligase catalysis. Dependence on ATP levels and modifier subunit for regulation of tissue glutathione levels. *J Biol Chem*. 2005;280:33766–33774.
17. **Zuelke KA, Jeffay SC, Zucker RM, Perreault SD.** Glutathione (GSH) concentrations vary with the cell cycle in maturing hamster oocytes, zygotes, and pre-implantation stage embryos. *Mol Reprod Dev*. 2003;64:106–112.
18. **Hirshfield AN.** Size-frequency analysis of atresia in cycling rats. *Biol Reprod*. 1988;38:1181–1188.
19. **Gosden RG, Laing SC, Felicio LS, Nelson JF, Finch CE.** Imminent oocyte exhaustion and reduced follicular recruitment mark the transition to acyclicity in aging C57BL/6J mice. *Biol Reprod*. 1983;28: 255–260.
20. **van Noord PAH, Boersma H, Dubas JS, te Velde ER, Dorland M.** Age at natural menopause in a population-based screening cohort: the role of menarche, fecundity, and lifestyle factors. *Fertil Steril*. 1997;68:95–102.
21. **Rebar RW.** Mechanisms of premature menopause. *Endocrinol Metab Clin North Am*. 2005;34:923–933.
22. **Nelson LM.** Primary ovarian insufficiency. *N Engl J Med*. 2009; 360:606–614.
23. **Sullivan SD, Castrillon DH.** Insights into primary ovarian insufficiency through genetically engineered mouse models. *Sem Reprod Med*. 2011;29:283–298.
24. **John GB, Gallardo TD, Shirley LJ, Castrillon DH.** Foxo3 Is a PI3K-dependent molecular switch controlling the initiation of oocyte growth. *Dev Biol*. 2008;321:197–204.
25. **Castrillon DH, Miao L, Kollipara R, Horner JW, DePinho RA.** Suppression of ovarian follicle activation in mice by the transcription factor Foxo3a. *Science*. 2003;301:215–218.
26. **Zheng W, Nagaraju G, Liu Z, Liu K.** Functional roles of the phosphatidylinositol 3-kinases (PI3Ks) signaling in the mammalian ovary. *Mol Cell Endocrinol*. 2012;356:24–30.
27. **Zhang H, Zheng W, Shen Y, Adhikari D, Ueno H, Liu K.** Experimental evidence showing that no mitotically active female germline progenitors exist in postnatal mouse ovaries. *Proc Natl Acad Sci USA*. 2012;109:12580–12585.
28. **Reddy P, Liu L, Adhikari D, et al.** Oocyte-specific deletion of *Pten* causes premature activation of the primordial follicle pool. *Science*. 2008;319:611–613.
29. **Reddy P, Adhikari D, Zheng W, et al.** PDK1 Signaling in oocytes controls reproductive aging and lifespan by manipulating the survival of primordial follicles. *Hum Mol Genet*. 2009;18:2813–2824.
30. **Cortés-Wanstreet MM, Giedzinski E, Limoli CL, Luderer U.** Overexpression of glutamate cysteine ligase protects human COV434 granulosa tumor cells against oxidative and γ-radiation-induced cell death. *Mutagenesis*. 2009;24:211–224.
31. **Tsai-Turton M, Luong BT, Tan Y, Luderer U.** Cyclophosphamide-induced apoptosis in COV434 human granulosa cells involves oxidative stress and glutathione depletion. *Toxicol Sci*. 2007;98:216–230.
32. **Tsai-Turton M, Nakamura BN, Luderer U.** Induction of apoptosis by 9,10-dimethyl-1,2-benzanthracene (DMBA) in cultured preovulatory rat follicles is preceded by a rise in reactive oxygen species and is prevented by glutathione. *Biol Reprod*. 2007;77:442–451.
33. **Tsai-Turton M, Luderer U.** Opposing effects of glutathione depletion and FSH on reactive oxygen species and apoptosis in cultured preovulatory rat follicles. *Endocrinology*. 2006;147:1224–1236.
34. **Lim J, Luderer U.** Oxidative damage increases and antioxidant gene expression decreases with aging in the mouse ovary. *Biol Reprod*. 2011;84:775–782.
35. **Tarín JJ.** Potential effects of age-associated oxidative stress on mammalian oocytes/embryos. *Mol Hum Reprod*. 1996;2:717–724.
36. **Pan H, Ma P, Zhu W, Schultz RM.** Age-associated increase in aneuploidy and changes in gene expression in mouse eggs. *Dev Biol*. 2008;316:397–407.
37. **Hamatani T, Falco G, Carter MG, et al.** Age-associated alteration of gene expression patterns in mouse oocytes. *Hum Mol Genet*. 2004; 13:2263–2278.
38. **Wiener-Megnazi Z, Vardi L, Lissak A, et al.** Oxidative stress indices in follicular fluid as measured by the thermochemi-luminescence

assay correlate with outcome parameters in in vitro fertilization. *Fertil Steril*. 2004;82(suppl 3):1171–1176.
39. **Tatone C, Carbone MC, Falone S, et al.** Age-dependent changes in the expression of superoxide dismutases and catalase are associated with ultrastructural modifications in human granulosa cells. *Mol Reprod Dev*. 2006;12:655–660.
40. **Das S, Chattopadhyay R, Ghosh S, et al.** Reactive oxygen species level in follicular fluid—embryo quality marker in IVF? *Hum Reprod*. 2006;21:2403–2407.
41. **Dalton TP, Dieter MZ, Yang Y, Shertzer HG, Nebert DW.** Knockout of the mouse glutamate cysteine ligase catalytic subunit (Gclc) gene: embryonic lethal when homozygous, and proposed model for moderate glutathione deficiency when heterozygous. *Biochem Biophys Res Commun*. 2000;279:324–329.
42. **Shi Z-Z, Osei-Frimpong J, Kala G, et al.** Glutathione synthesis is essential for mouse development but not for cell growth in culture. *Proc Natl Acad Sci USA*. 2000;97:5101–5106.
43. **Giordano G, White CC, McConnachie LA, Fernandez C, Kavanagh TJ, Costa LG.** Neurotoxicity of domoic acid in cerebellar granule neurons in a genetic model of glutathione deficiency. *Mol Pharmacol*. 2006;70:2116–2126.
44. **Yang Y, Dieter MZ, Chen Y, Shertzer HG, Nebert DW, Dalton TP.** Initial characterization of the glutamate cysteine ligase modifier subunit *Gclm (−/−)* knockout mouse: novel model system for severely compromised oxidative stress response. *J Biol Chem*. 2002;277:49446–49452.
45. **Nakamura BN, Fielder TJ, Hoang YD, et al.** Lack of maternal glutamate cysteine ligase modifier subunit (*Gclm*) decreases oocyte glutathione concentrations and disrupts preimplantation development in mice. *Endocrinology*. 2011;152:2806–2815.
46. **McConnachie LA, Mohar I, Hudson FN, et al.** Glutamate cysteine ligase modifier subunit deficiency and gender as determinants of acetaminophen-induced hepatotoxicity in mice. *Toxicol Sci*. 2007;99:628–636.
47. **National Research Council.** *Guide for the Care and Use of Laboratory Animals*. Washington, DC: National Research Council, National Academy of Sciences; 1996.
48. **Cooper RL, Goldman JM, Vandenbergh JG.** Monitoring of the estrous cycle in the laboratory rodent by vaginal lavage. In: Heindel JJ, Chapin RE, eds. *Female Reproductive Toxicology*. San Diego: Academic Press, Inc; 1993:45–55.
49. **McClintock MK.** Social control of the ovarian cycle and the function of estrous synchrony. *Am Zool*. 1981;21:243–256.
50. **Griffith OW.** Determination of glutathione and glutathione disulfide using glutathione reductase and 2-vinylpyridine. *Anal Biochem*. 1980;106:207–212.
51. **Tsai-Turton M, Luderer U.** Gonadotropin regulation of glutamate cysteine ligase catalytic and modifier subunit expression in the rat ovary is subunit and follicle stage-specific. *Am J Physiol*. 2005;289:E391–E402.
52. **Jones DP.** Redox potential of GSH/GSSG couple: assay and biological significance. *Methods Enzymol*. 2002;348:93–112.
53. **Jones DP, Mody VCJ, Carlson JL, Lynn MJ, Sternberg PJ.** Redox analysis of human plasma allows separation of pro-oxidant events of aging from decline in antioxidant defenses. *Free Radic Biol Med*. 2002;33:1290–1300.
54. **FitzHarris G, Baltz JM.** Regulation of intracellular pH during oocyte growth and maturation in mammals. *Reproduction*. 2009;138:619–627.
55. **Lopez SG, Luderer U.** Effects of cyclophosphamide and buthionine sulfoximine on ovarian glutathione and apoptosis. *Free Radic Biol Med*. 2004;36:1366–1377.
56. **Pedersen T, Peters H.** Proposal for a classification of oocytes in the mouse ovary. *J Reprod Fertil*. 1968;17:555–557.
57. **Plowchalk DR, Smith BJ, Mattison DR.** Assessment of toxicity to the ovary using follicle quantitation and morphometrics. In: Heindel JJ, Chapin RE, eds. *Female Reproductive Toxicology*. San Diego: Academic Press; 1993:57–68.
58. **Desmeules P, Devine PJ.** Characterizing the ovotoxicity of cyclophosphamide metabolites on cultured mouse ovaries. *Toxicol Sci*. 2006;90:500–509.
59. **Pepling ME.** From primordial germ cell to primordial follicle: mammalian female germ cell development. *Genesis*. 2006;44:622–632.
60. **Canning J, Takai Y, Tilly JL.** Evidence for genetic modifiers of ovarian follicular endowment and development from studies of five inbred mouse strains. *Endocrinology*. 2002;144:9–12.
61. **Lim J, Lawson GW, Nakamura BN, et al.** Glutathione-deficient mice have increased sensitivity to transplacental benzo[a]pyrene-induced premature ovarian failure and ovarian tumorigenesis. *Cancer Res*. 2013;73:908–917.
62. **Pasternack BS, Shore RE.** Analysis of dichotomous response data from toxicological experiments involving stable laboratory mouse populations. *Biometrics*. 1982;38:1057–1067.
63. **Devine PJ, Payne CM, McCuskey MK, Hoyer PB.** Ultrastructural evaluation of oocytes during atresia in rat ovarian follicles. *Biol Reprod*. 2000;63:1245–1252.
64. **Tingen CM, Bristol-Gould SK, Kiesewetter SE, Wellington JT, Shea L, Woodruff TK.** Prepubertal primordial follicle loss in mice is not due to classical apoptotic pathways. *Biol Reprod*. 2009;81:16–25.
65. **Nakamura BN, Mohar I, Lawson GW, et al.** Increased sensitivity to testicular toxicity of transplacental benzo[a]pyrene exposure in male glutamate cysteine ligase modifier subunit *Gclm−/−)* knockout mice. *Toxicol Sci*. 2012;126:227–241.
66. **Rebrin I, Kamzalov S, Sohal RS.** Effects of age and caloric restriction on glutathione redox state in mice. *Free Radic Biol Med*. 2003;35:626–635.
67. **Rebrin I, Forster MJ, Sohal RS.** Effects of age and caloric intake on glutathione redox state in different brain regions of C57BL/6 and DBA/2 mice. *Brain Res*. 2007;1127:10–18.
68. **Dean RT, Gieseg S, Davies MJ.** Reactive species and their accumulation on radical-damaged proteins. *Trends Biochem Sci*. 1993;18:437–441.
69. **Halliwell B.** Antioxidant characterization. Methodology and mechanism. *Biochem Pharmacol*. 1995;49:1341–1348.
70. **Knight TR, Kurtz A, Bajt ML, Hinson JA, Jaeschke H.** Vascular and hepatocellular peroxynitrite formation during acetaminophen toxicity: role of mitochondrial oxidant stress. *Toxicol Sci*. 2001;62:212–220.
71. **van der Vliet A, Eiserich JP, Shigenaga MK, Cross CE.** Reactive nitrogen species and tyrosine nitration in the respiratory tract: epiphenomena or a pathobiologic mechanism of disease? *Am J Respir Crit Care Med*. 1999;160:1–9.
72. **Beckman JS, Koppenol WH.** Nitric oxide, superoxide, and peroxynitrite: the good, the bad, and the ugly. *Am J Physiol*. 1996;271:C1424–C1437.
73. **Uda M, Ottolenghi C, Crisponi L, et al.** Foxl2 disruption causes mouse ovarian failure by pervasive blockage of follicle development. *Hum Mol Genet*. 2004;13:1171–1181.
74. **Schmidt D, Ovitt CE, Anlag K, et al.** The murine winged-helix transcription factor Foxl2 is required for granulosa cell differentiation and ovary maintenance. *Development*. 2004;131:933–942.
75. **Zhang X, Tang N, Hadden TJ, Rishi AK.** Akt, Foxo and regulation of apoptosis. *Biochim Biophys Acta*. 2011;1813:1978–1986.
76. **LaHair MM, Howe CJ, Rodriguez-Mora O, McCubrey JA, Franklin RA.** Molecular pathways leading to oxidative stress-induced phosphorylation of Akt. *Antiox Redox Signal*. 2006;8:1749–1756.
77. **King SM, Quartuccio SM, Vanderhyden BC, Burdette JE.** Early transformative changes in normal ovarian surface epithelium induced by oxidative stress require Akt upregulation, DNA damage and epithelial-stromal interaction. *Carcinogenesis*. 2013;34:1125–1133.
78. **Rodrigues P, Limback D, McGinnis LK, Plancha CE, Albertini DF.**

Multiple mechanisms of germ cell loss in the perinatal mouse ovary. *Reproduction*. 2009;137:709–720.
79. **Gannon AM, Stämpfli MR, Foster WG.** Cigarette smoke exposure leads to follicle loss via an alternative ovarian cell death pathway in a mouse model. *Toxicol Sci*. 2012;125:274–284.
80. **Chan JY, Kwong M.** Impaired expression of glutathione synthetic enzyme genes in mice with targeted deletion of the Nrf2 basic-leucine zipper protein. *Biochim Biophys Acta*. 2000;1517:19–26.
81. **Ramos-Gomez M, Kwak M-K, Dolan PM, et al.** Sensitivity to carcinogenesis is increased and chemoprotective efficacy of enzyme inducers is lost in *nrf2* transcription factor-deficient mice. *Proc Natl Acad Sci USA*. 2001;98:3410–3415.
82. **Hu X, Roberts JR, Apopa PL, Kan YW, Ma Q.** Accelerated ovarian failure induced by 4-vinyl cyclohexene diepoxide in Nrf2 null mice. *Mol Cell Biol*. 2006;26:940–954.
83. **Matzuk MM, Dionne L, Guo Q, Kumar TR, Lebovitz RM.** Ovarian function in superoxide dismutase 1 and 2 knockout mice. *Endocrinology*. 1998;139:4008–4011.
84. **Ho Y-S, Gargano M, Cao J, Bronson RT, Heimler I, Hutz RJ.** Reduced fertility in female mice lacking copper-zinc superoxide dismutase. *J Biol Chem*. 1998;273:7765–7769.
85. **Wong PC, Waggoner D, Subramaniam JR, et al.** Copper chaperone for superoxide dismutase is essential to activate mammalian Cu/Zn superoxide dismutase. *Proc Natl Acad Sci USA*. 2000;97:2886–2891.
86. **Kumar TR, Wiseman AL, Kala G, Kala SV, Matzuk MM, Lieberman MW.** Reproductive defects in γ-glutamyl transpeptidase deficient mice. *Endocrinology*. 2000;141:4270–4277.
87. **Lieberman MW, Wiseman AL, Shi Z-Z, et al.** Growth retardation and cysteine deficiency in γ-glutamyl transpeptidase-deficient mice. *Proc Natl Acad Sci USA*. 1996;93:7923–7926.
88. **Will Y, Fishcher KA, Horton RA, et al.** γ-Glutamyltranspeptidase-deficient knockout mice as a model to study the relationship between glutathione status, mitochondrial function, and cellular function. *Hepatology*. 2000;32:740–749.
89. **Ho Y-S, Magnenat J-L, Bronson RT, et al.** Mice deficient in cellular glutathione peroxidase develop normally and show no increased sensitivity to hyperoxia. *J Biol Chem*. 1997;272:16644–16651.
90. **Ho Y-S, Xiong Y, Ma W, Spector A, Ho DS.** Mice lacking catalase develop normally but show differential sensitivity to oxidant tissue injury. *J Biol Chem*. 2004;279:32804–32812.